Title:

Pannexin 1 Channels Control Cardiomyocyte Metabolism and Neutrophil Recruitment During Non-Ischemic Heart Failure

Caitlin M. Pavelec[1,3], Alexander P. Young[2,3], Hannah L. Luviano[1], Emily E. Orrell[1], Nabin Poudel[4], Abigail G. Wolpe[5], Samantha H. Thomas[1], Scott Yeudall[1], Clint M. Upchurch[1], Mark D. Okusa[4], Brant E. Isakson[3,7], Matthew J. Wolf[2,3], Norbert Leitinger[1,3]

Affiliations

1. Department of Pharmacology, University of Virginia School of Medicine, Charlottesville, VA
2. Cardiovascular Medicine, Department of Medicine, University of Virginia School of Medicine, Charlottesville, VA
3. Robert M. Berne Cardiovascular Research Center, University of Virginia School of Medicine, Charlottesville, VA
4. Division of Nephrology and Center for Immunity, Inflammation and Regenerative Medicine, University of Virginia School of Medicine, Charlottesville, VA
5. Department of Cell Biology, University of Virginia School of Medicine, Charlottesville, VA
6. Department of Molecular Physiology and Biophysics, University of Virginia School of Medicine, Charlottesville, VA

Funding:

This work was supported by NIH P01 HL120840 (to N.L., B.E.I.), NIH T32 HL007284 (to C.M.P.), NIH F31HL165918-01A1 (to C.M.P.), NIH F31 HL149221 to (to A.G.W.), NIH R01 HL137112 (to B.E.I.), NIH F30 HL154554-01 (to S.Y.), NIH T32 GM007055 (to S.Y., C.M.U.), NIH T32 GM007267 (to S.Y.), NIH R01 HL162925 (to M.J.W.),NIH R01 DK085259 (to M.D.O.), NIH R01 DK123248 (to M.D.O.), the summer research internship program at the University of Virginia (to S.H.T), University of Virginia Office of Citizen Scholar Development Double Hoo Award (to H.L.L., to C.M.P.).

Acknowledgements:

We thank the members of the Pannexin Interest Group for their input and expertise throughout the project. We thank the Cardiovascular Research Center histology core, and the Flow Cytometry Core Facility at the University of Virginia School of Medicine for their expertise and resources.

Abstract:

Pannexin 1 (PANX1), a ubiquitously expressed ATP release membrane channel, has been shown to play a role in inflammation, blood pressure regulation, and myocardial infarction. However, a possible role of PANX1 in cardiomyocytes in the progression of heart failure has not yet been investigated. We generated a novel mouse line with constitutive deletion of PANX1 in cardiomyocytes ($Panx1^{MyHC6}$). PANX1 deletion in cardiomyocytes had no effect on unstressed heart function but increased the glycolytic metabolism both *in vivo* and *in vitro*. *In vitro*, treatment of H9c2 cardiomyocytes with isoproterenol led to PANX1-dependent release of ATP and Yo-Pro-1 uptake, as assessed by pharmacological blockade with spironolactone and siRNA-mediated knock-down of PANX1. To investigate non-ischemic heart failure and the preceding cardiac hypertrophy we administered isoproterenol, and we demonstrate that $Panx1^{MyHC6}$ mice were protected from systolic and diastolic left ventricle volume increases and cardiomyocyte hypertrophy. Moreover, we found that $Panx1^{MyHC6}$ mice showed decreased isoproterenol-induced recruitment of immune cells ($CD45^+$), particularly neutrophils ($CD11b^+$, $Ly6g^+$), to the myocardium. Together these data demonstrate that PANX1 deficiency in cardiomyocytes impacts glycolytic metabolism and protects against cardiac hypertrophy in non-ischemic heart failure at least in part by reducing immune cell recruitment. Our study implies PANX1 channel inhibition as a therapeutic approach to ameliorate cardiac dysfunction in heart failure patients.

54 Introduction

55 Heart failure, which affects five million Americans each year and has a five-year survival
56 rate of less than 50 percent[1], can be divided in to two sub-pathologies: heart failure with reduced
57 ejection fraction (HFrEF) and heart failure with preserved ejection fraction (HFpEF); HFpEF is the
58 more predominant form and its prevalence is on the rise[1,2]. While several effective therapies are
59 available for patients with HFrEF, HFpEF has limited treatment options underscoring the need to
60 identify new therapeutic strategies[3]. Pathological features of heart failure include cardiac
61 hypertrophy, chronic inflammation, and interstitial fibrosis of the heart muscle, which together
62 result in reduced cardiac contractile function[4]. Current pharmacologic interventions for HFrEF
63 include treatments with beta-blockers, loop diuretics, angiotensin converting enzyme (ACE)
64 inhibitors, angiotensin receptor blockers, and sodium glucose transporter 2 (SGLT2) inhibitors[4–6].
65 These therapies target the renin-angiotensin/ aldosterone systems and the adrenergic signaling
66 axes, providing more symptom management than improving function of the cardiac muscle[5].
67 Moreover, previous clinical trials that have targeted TNF-α signaling, modulated the immune
68 system using intravenous immunoglobulins[7], or decreased fibroblast activation with pirfenidone[8]
69 (an antifibrotic which down regulates growth factors and procollagens I and II), have not lead to
70 significant improvements in patient outcomes. To prevent cardiac muscle decline, it is necessary
71 to devise novel therapeutic approaches which directly target the mechanisms of heart failure
72 progression.

73 Proper contractile function of the heart requires, at the level of the cardiomyocyte,
74 sufficient cellular energy in the form of accessible ATP[9,10]. Adult cardiomyocytes rely on fatty acids
75 as their main fuel source to generate ATP, but they are metabolically flexible and can use glucose,

76 branched-chain amino acids, or ketones as needed[11]. During heart failure, cardiomyocytes
77 demonstrate an increased demand for ATP due to more frequent but less effective contraction[12].
78 In order to meet this increased energy demand, cardiomyocytes shift their metabolism from
79 utilizing fatty acids to utilizing glucose, which is accompanied by increased glycolysis[13], which
80 resembles the reliance on glucose and glycolysis in fetal cardiomyocytes[11,14]. Moreover, recent
81 work has demonstrated that decreased reliance on fatty acid oxidation confers greater resistance
82 to ischemia reperfusion injury and promotes cardiomyocyte proliferation in mice deficient in the
83 mitochondrial fatty acid transporter *Cpt1b*[15]. These findings suggest that a metabolic shift to
84 glucose utilization by cardiomyocytes protects against cardiac injury.

85 In response to local hypoxia or chronic beta-adrenergic stimulation, two conditions known
86 to cause cardiac hypertrophy and heart failure, cardiomyocytes release damage signals such as
87 ATP[16] and secrete pro-inflammatory cytokines, which leads to the recruitment of macrophages
88 and neutrophils and efferocytosis of dying cardiomyocytes[7,17]. Initially, recruited leukocytes
89 promote the repair of damaged myocardium by stimulating resident fibroblasts to secrete
90 extracellular matrix, and by inducing angiogenesis to provide needed oxygenation and nutrients
91 to the healing cardiac muscle[18,19]. While this acute inflammatory response is necessary to activate
92 fibroblasts and prevent excessive cardiomyocyte death, chronic activation of both the innate and
93 adaptive immune responses has been shown to exacerbate heart failure progression[7,20–22]. The
94 immune cell cascade and timeline for resolution of inflammation after ischemic myocardial
95 infarction has been well characterized, however, it is less well understood how immune cells are
96 recruited to the injured myocardium in chronically developing non-ischemic heart failure[23].

97 Pannexin 1 (PANX1) is a ubiquitously expressed transmembrane channel, through which
98 stressed or damaged cells release ATP and other small metabolites that are smaller than 1 kDa.
99 PANX1-dependent ATP release from apoptotic cells serves as a "find me" signal for efferocytosis
100 by immune cells[24–26]. PANX1 channel opening can be activated via multiple mechanisms including
101 α_{1D}[27]- or β-adrenergic receptor stimulation[28,29], and caspase-3-mediated cleavage[30]. Several
102 pharmacologic compounds including probenecid, carbenoxolone, and the FDA-approved heart
103 failure therapeutic spironolactone have been identified as PANX1 channel blockers[31–33]. Release
104 of ATP from cardiomyocytes through PANX1, which caused fibroblast activation *in vitro,* has
105 previously been described[16]. Moreover, global PANX1 deletion in mice decreased ischemic area
106 in a model of cardiac ischemia reperfusion injury[34], while endothelial cell-specific deletion of
107 PANX1 in mice decreased immune cell infiltration in a model of myocardial infarction[35]. While
108 these prior studies have strongly implied PANX1 as a therapeutic target for cardiovascular
109 diseases in general[36], the role for PANX1 in cardiomyocytes specifically in the regulation of
110 chronic cardiac pathologies, including heart failure, remains to be elucidated.

111 Here we report that PANX1 channels can be activated in cardiomyocytes through beta-
112 adrenergic receptor stimulation. Using mice with a cardiomyocyte-specific PANX1 deletion
113 ($Panx1^{MyHC6}$), we demonstrate a crucial role for PANX1 channels in the development of non-
114 ischemic heart failure. $Panx1^{MyHC6}$ mice were protected against isoproterenol-induced [37,38] cardiac
115 hypertrophy, systolic dysfunction, and neutrophil infiltration into the myocardium. Furthermore,
116 we find that PANX1 deletion facilitates glucose utilization and increases glycolytic and decreases
117 inflammatory gene expression. Taken together our findings implicate PANX1 channels as
118 promising therapeutic targets in non-ischemic heart failure and cardiac hypertrophy.

119 **Results:**

120 **Isoproterenol Activates Pannexin 1 channels in Cardiomyocytes:**

121 Previous studies have demonstrated that Pannexin 1 (PANX1) channels are activated in
122 response to β3 and α_{1D}-adrenergic receptor stimuli[27,28]. A recent study demonstrates beta-
123 adrenergic receptor 1-dependent activation of Panx1 channels in cardiomyocytes via cAMP/PKA-
124 mediated phosphorylation on Serine 206[29]. To activate Panx1 channels we used isoproterenol, a
125 pan β-adrenergic receptor agonist, in H9c2 rat myoblasts which endogenously express all β-
126 adrenergic receptor family members and Panx1[39–41]. We tested Panx1 channel opening by
127 measuring both ATP release into the culture media and dye (Yo-Pro-1) uptake into cells. After
128 stimulation with 2 or 20µM isoproterenol, H9c2 cells released significantly more ATP into the
129 extracellular media compared to vehicle stimulation (**Figure 1A**). Isoproterenol-induced ATP
130 release was abolished by either siRNA mediated knock-down of Panx1 (successful knock-down is
131 demonstrated by significantly decreased mRNA and protein levels (S1A,B)), or pharmacological
132 channel inhibition with spironolactone[33] (**Figure 1A,C**). Cell viability was not affected at either
133 dose of isoproterenol (S1C).

134 Additionally, using a flow-cytometry based approach, we found that stimulation with
135 20µM isoproterenol caused a significant increase in Yo-Pro-1 positive, Annexin V negative H9c2
136 cells compared with vehicle stimulation (**Figure 1B**, representative gating S1D). Isoproterenol-
137 induced Yo-Pro-1 uptake was significantly decreased after siRNA-mediated Panx1 knock-down
138 (**Figure 1B,** S1D), and blunted with PANX1 channel blockade by spironolactone, carbenoxolone,
139 or probenecid (**Figure 1D**). Taken together, these data demonstrate that PANX1 channel opening
140 in cardiac myoblasts as a result of β-adrenergic receptor stimulation leads to the release of ATP.

141 **Generation and characterization of a mouse with Pannexin 1 deletion specifically in**
142 **cardiomyocytes**

143 To investigate the role of PANX1 channels in cardiomyocytes *in vivo*, we generated a
144 cardiomyocyte-specific PANX1 null mouse by crossing Panx1 floxed mice[42] with mice expressing
145 Cre recombinase under the control of the alpha myosin heavy chain promoter (MyHC6).
146 Confirmation of successful recombination was demonstrated by the presence of a null band on
147 PCR analysis of genomic DNA isolated from the hearts of Panx1^{MyHC6} mice, which was not present
148 in the hearts of Panx1$^{fl/fl}$ mice or other tested organs (liver, kidney) from either mouse genotype
149 (S2A). Levels of *Panx1* mRNA (by qPCR) and PANX1 protein (by immunofluorescence) were
150 significantly decreased in isolated cardiomyocytes and cardiac troponin t (cTnnt) positive cells,
151 respectively, from Panx1^{MyHC6} mice (**Figure 2A**, S2B). Panx1^{MyHC6} mice had no obvious gross
152 developmental defects when compared to their Panx1$^{fl/fl}$ littermates as examined by body mass,
153 organ mass, or tibial length at 12 weeks of age (S2C-F). Furthermore, assessment of cardiac
154 function via 2D-echocardiography showed no significant differences in end-systolic or end-
155 diastolic volume, wall thickness, or ejection fraction at baseline (**Figure 2B-E,** S2K). Finally, blood
156 pressure measurements by radiotelemetry in 12-week-old male mice demonstrated no
157 differences in mean arterial pressure, systolic or diastolic pressure, or heart rate in Panx1^{MyHC6}
158 mice when compared to littermate Panx1$^{fl/fl}$ mice (S2G-J).

159 **Pannexin 1 deletion shifts cardiomyocyte metabolism from oxidative phosphorylation to**
160 **glycolysis.**

161 To explore effects of PANX1 deficiency on the cardiomyocyte transcriptome *in vivo*, we
162 performed bulk RNA-sequencing on cardiomyocytes isolated from hearts of Panx1^{MyHC6} and

163 Panx1$^{fl/fl}$ mice, which identified 1281 and 727 uniquely expressed genes, respectively (**Figure 3A)**.
164 There were 1069 significantly differentially expressed genes between the genotypes, with 793
165 down-regulated and 276 up-regulated (**Figure 3B**). Gene ontology (GO) Term and KEGG pathway
166 analysis revealed that Panx1 deletion mainly affected pathways involved in intercellular
167 communication, cell adhesion and gap junction function, namely "cell-cell" and "Wnt signaling",
168 "microtubule-based movement", "ECM-receptor interactions", "leukocyte trans endothelial
169 migration", and "cell adhesion molecules", among others involved in inflammation and
170 cytoskeletal organization (S3A, B). KEGG Pathway analysis was corroborated by significantly lower
171 expression of transcripts of the claudin and cadherin family and their receptors (*Cdh1, Cldn7,*
172 *Cdhr3, Cdhr4*), as well as increased expression of Transport and Golgi Organization protein 2
173 Homolog (*Tango2*) , which has been associated with altered mitochondrial energy metabolism in
174 humans[43,44] (**Figure 3B)**.

175 Pannexin channels have been demonstrated to control cellular metabolism, specifically
176 the regulation of glucose homeostasis and glycolytic metabolism[45–48]. A previous study by
177 Adamson et al. demonstrated that Panx1 channel function is required for insulin-induced glucose
178 metabolism in white adipocytes[49]. To assess whether loss of PANX1 impacted these pathways in
179 cardiomyocytes, we analyzed the genes associated with key glycolytic enzymes in PANX1-
180 deficient cardiomyocytes. Our data demonstrate increased expression of glycolytic pathway
181 genes in cardiomyocytes isolated from Panx1^{MyHC6} mice compared to their floxed controls. Of
182 note, we found a significantly higher levels of the glucose transporter *Slc2a4* (Glut4), which is the
183 predominant isoform in cardiomyocytes (**Figure 3C**).

184 To determine if the observed transcriptional increase in genes involved in glycolysis
185 impacts cellular metabolism and glucose utilization, we first performed a glycolytic stress test
186 (GST) using a Seahorse extracellular flux analyzer on H9c2 cells that had been treated with either
187 Panx1 siRNA or control siRNA. PANX1 knock-down alone resulted in significantly increased basal
188 and maximal extracellular acidification rate (ECAR). The magnitude of increase was even further
189 increased by treatment with isoproterenol (**Figures 3D, E,** representative trace S3C).

190 Next, we performed glucose uptake assays to determine if the increase in glycolytic rate
191 shown in the glycolytic stress test could be attributed to an increase in glucose present in the
192 cardiomyocyte. Intracellular 2NBD-glucose levels were significantly increased after stimulation of
193 H9c2 cells with isoproterenol, which was abrogated after siRNA-mediated knock down of PANX1
194 (**Figure 3F**). Though cardiomyocyte metabolism was significantly changed by PANX1 deletion *in*
195 *vitro*, intracellular ATP content is not significantly different (S3D). Taken together these data
196 demonstrate a key role for PANX1 channels in regulating glucose uptake and glycolytic rate in
197 H9c2 cardiomyocytes.

198 **Panx1 deficiency in cardiomyocytes protects against isoproterenol-induced cardiac**
199 **hypertrophy and cardiac dysfunction in non-ischemic heart failure**

200 To examine the role of Panx1 channels in regulating cardiomyocyte function of the heart
201 under stress, we induced cardiac hypertrophy preceding non-ischemic heart failure using an
202 established protocol where we repeatedly administered isoproterenol via intraperitoneal
203 injection for 14 days at a dose of 15mg/kg/day[37,50]. We established this timepoint as an early
204 measure of disease progression, where cardiac hypertrophy is the predominate phenotype. We
205 performed 2D-echocardiography prior to the beginning of the study to collect baseline

206 measurements and then again after 14 days at the model endpoint (**Figure 4A**). As shown
207 previously, before the start of the treatment Panx1$^{fl/fl}$ and Panx1^{MyHC6} mice displayed no overt
208 differences in cardiac function (Figure 2B-E) or weight (S4A). Repeated isoproterenol
209 administration resulted in significantly increased heart weight in Panx1$^{fl/fl}$ mice, but not in
210 Panx1^{MyHC6} mice (**Figure 4B,** S4B). Cardiomyocyte hypertrophy (as measured by cardiomyocyte
211 cross sectional area by wheat germ agglutinin (WGA) staining) was significantly increased in
212 hearts of in Panx1$^{fl/fl}$ mice compared with Panx1^{MyHC6} mice after isoproterenol treatment (**Figure**
213 **4C**).

214 Furthermore, treatment with isoproterenol caused significant increases in both end-
215 systolic and end-diastolic volume of the left ventricle in Panx1$^{fl/fl}$ mice as measured by
216 echocardiography (**Figure 4D-F,** S4G). Panx1^{MyHC6} mice did not have significant increases in either
217 metric compared to their baseline and had significant less change compared to Panx1$^{fl/fl}$ age and
218 sex-matched controls (**Figure 4D-F,** S4G). We determined that this disparity was likely caused by
219 heart-intrinsic functional defects and not systemic vascular or renal damage, as we observed no
220 differences in blood pressure or serum creatinine between Panx1$^{fl/fl}$ and Panx1^{MyHC6} mice after
221 treatment with isoproterenol (S4C-F).

222 Additionally, to assess cardiac fibrosis found at later stages of non-ischemic heart failure
223 and to examine if Panx1 deficiency would also protect against fibrotic changes, we induced non-
224 ischemic heart failure by administration of isoproterenol for 28 days (15/mg/kg/day) by
225 subcutaneous implantation of osmotic pump (S5A). Prolonged isoproterenol treatment caused a
226 significantly greater increase in Collagen 1 (COL1A1) content in the myocardium of Panx1$^{fl/fl}$ mice
227 compared to Panx1^{MyHC6} mice, as determined by immunofluorescence staining (S5B).

228 These data demonstrate that cardiomyocyte-specific deletion of PANX1 is
229 cardioprotective against cardiac hypertrophy and interstitial fibrosis during the progression of
230 non-ischemic heart failure.

231 **Pathways involved in the immune response and fatty-acid metabolism are down regulated in**
232 **the hearts of Panx1^{MyHC6} mice during non-ischemic heart failure**

233 To elucidate potential mechanisms that are involved in the protection from cardiac
234 hypertrophy and dysfunction observed in Panx1^{MyHC6} mice, we performed bulk RNA-sequencing
235 on whole hearts of Panx1$^{fl/fl}$ and Panx1^{MyHC6} mice after 14-day administration of isoproterenol.
236 We identified 1592 genes which were significantly differentially expressed between the two
237 genotypes, with 594 genes downregulated and 998 upregulated in Panx1^{MyHC6} mice compared to
238 Panx1$^{fl/fl}$ controls (**Figure 5A**).

239 KEGG pathway and GO Term analysis on the differentially expressed genes identified
240 regulatory pathway families including “hematopoietic cell lineage”, “cell adhesion molecules”, “B-
241 cell receptor signaling pathway”, and “Rheumatoid arthritis”, all of which suggested significant
242 changes in molecules associated with immune cell recruitment and infiltration. Moreover, we
243 identified “fatty acid degradation”, “fatty acid metabolism”, and “cardiac muscle contraction”,
244 implicating a metabolic shift in the absence of PANX1 channels. Furthermore, identified GO Terms
245 indicated changes in plasma membrane proteins, specifically transporters and ion channels, as
246 well as “oxidoreductase activity”, “scavenger receptor activity”, and “hydrolase activity”,
247 implicating the possible shift in the oxidative stress state.

248 Further analysis of genes associated with fatty acid beta-oxidation (as identified through
249 WikiPathways) demonstrated overall decreased expression of this group of genes in hearts from

250 Panx1^{MyHC6} mice with non-ischemic heart failure, while some genes such as *Lipc* (encoding the
251 lipase C hepatic type), were expressed at higher levels (**Figure 5B**). Interestingly, a lowered
252 reliance on fatty acid beta-oxidation during ischemic stress has been previously associated with
253 increased cardiomyocyte viability[15].

254 Examination of genes involved in the inflammatory response identified lower expression
255 of *Cd40*, *Il2ra*, and *Il2* in hearts of Panx1^{MyHC6} mice compared to their Panx1$^{fl/fl}$ counterparts
256 (**Figure 5C**), suggesting a lower immune cell load in the hearts as CD40 and IL-2 expression are
257 associated with a wide range of leukocyte populations[51]. Additionally, we observed lower
258 expression of *Lamb1* (encoding Laminin subunit beta 1) and *Lama5* (encoding laminin subunit
259 alpha 5) as well as *Vtn* (encoding Vitronectin) suggestive of decreased cell-cell adhesion and
260 fibrosis (**Figure 5C**).

261 Since PANX1 channel function has been associated with activation of a variety of
262 purinergic receptors[29,52–54], we examined the expression of purinergic signaling receptors and
263 other associated molecular regulators in our RNA-Seq dataset (WikiPathway "Purinergic
264 signaling"). We found lower expression of *P2yr1*, *P2rx1*, *P2ry14,* and *Adora2a* in hearts of
265 Panx1^{MyHC6} mice (**Figure 5D**) compared to Panx1$^{fl/fl}$ controls. This finding is particularly interesting
266 as *P2rx1, P2yr14*, and *Adora2a* have all been previously associated with chemotaxis and activation
267 of immune cells, particularly neutrophils[55].

268 Together these data identify that PANX1 deficiency in cardiomyocytes causes significant
269 transcriptomic changes in genes associated with inflammation, immune cell recruitment,
270 metabolism and oxidative phosphorylation, all of which may contribute to the protection of

271 Panx1^{MyHC6} mice from cardiac hypertrophy and progressive heart failure in a model of
272 isoproterenol induced non-ischemic heart failure.

273 **Neutrophil infiltration is significantly blunted in Panx1^{MyHC6} mice during heart failure induced**
274 **by isoproterenol**

275 To determine the contribution of cardiomyocytes to the inflammatory state in
276 isoproterenol-injured hearts, we performed bulk RNA-Seq on the isolated cardiomyocytes from
277 Panx1$^{fl/fl}$ and Panx1^{MyHC6} mice. We identified 1439 differentially expressed genes with the majority
278 being downregulated in Panx1-deficient cardiomyocytes (1037 down, 402 up) (S6A). Further
279 analysis of genes associated with "inflammation response" (WikiPathways) revealed decreased
280 expression of many of the genes identified as being regulatory in inflammation including Zap70,
281 Lack, Fn1, Col1a2, and multiple cytokine receptors (**Figure 6A**). This was corroborated by the
282 finding of the GO Terms "immune response" and "immune system process", which were
283 significantly enriched with genes downregulated in the isolated cardiomyocyte fraction of
284 Panx1^{MyHC6} mice compared to Panx1$^{fl/fl}$ mice (**Figure 6A**).

285 To determine whether the observed inflammatory gene regulation patterns was reflective
286 of perturbed leukocyte recruitment to the hearts of Panx1^{MyHC6} mice, we isolated the non-
287 myocyte fractions from the hearts of Panx1$^{fl/fl}$ and Panx1^{MyHC6} mice after 14-day treatment with
288 isoproterenol and examined leukocyte populations by flow cytometry (representative gating S6B).
289 The number of total leukocytes (CD45^{+}) as well as neutrophils (Ly6g^{+}, CD11b^{+}) were significantly
290 lower in the hearts of Panx1^{MyHC6} mice (**Figure 6B, C,** S6B). These findings were confirmed by
291 immunofluorescence imaging of the left ventricle of hearts from Panx1$^{fl/fl}$ and Panx1^{MyHC6} mice.
292 In accordance with the flow cytometry data, the number of Ly6g^{+} puncta per field in the hearts

293 of Panx1^{MyHC6} mice was significantly lower compared to hearts from Panx1$^{fl/fl}$ mice (**Figure 6D,**
294 S6C).

295 Of note, there was no significant difference in the total number of macrophages (F4/80^{+},
296 CD11b^{+}) present in Panx1^{MyHC6} mouse hearts during non-ischemic heart failure (**Figure 6E,** S6D).
297 Further analysis of macrophage subsets showed no differences in macrophages with the co-
298 stimulatory macrophage activation marker CD86 (F4/80^{+}, CD11b^{+}, CD86^{+}) or macrophages with
299 the anti-inflammatory marker CD163 (F4/80^{+}, CD11b^{+}, CD163^{+}/CD86^{-}) (**Figure 6E,** S6D). Finally,
300 we observed no differences in dendritic cells (CD11b^{+}, CD24^{+}) (**Figure 6E,** S6D).

301 These data demonstrate a critical role for PANX1 expressed in cardiomyocytes in recruiting
302 immune cells, specifically neutrophils, to the myocardium in response to chronic beta-adrenergic
303 stimulation. This finding is in line with previous work which demonstrates that PANX1-dependent
304 ATP release recruits neutrophils to the endothelium during acute inflammatory disease[56].

305

306 **Discussion:**

307 The role of ATP, adenosine, and other purinergic signaling molecules as both autocrine
308 and paracrine signals in the myocardium has long been understood and exploited clinically, using
309 compounds such as clopidogrel and adenosine[57]. However, the underlying mechanisms for
310 release of purinergic compounds in non-ischemic heart failure still need to be investigated[58,59].

311 To examine the role of PANX1 in cardiomyocytes, we generated a novel mouse with
312 cardiomyocyte-specific deletion of PANX1 (Panx1^{MyHC6}). We found that Panx1^{MyHC6} mice shift the
313 baseline metabolic state of their cardiomyocytes toward a more glycolytic phenotype, concurrent
314 with increased glucose uptake and GLUT4 transporter expression. After isoproterenol-induced

315 non-ischemic heart failure, PANX1^{MyHC6} mice are protected from pathological cardiac hypertrophy
316 and dysfunction. We also find that in Panx1^{MyHC6} mouse hearts during isoproterenol-induced
317 cardiac hypertrophy there is a decrease in gene expression of fatty-acid beta oxidation- associated
318 genes. Finally, PANX1 deficiency in cardiomyocytes blunts neutrophil recruitment to the
319 myocardium during isoproterenol-induced non-ischemic heart failure.

320 Two previous studies by Adamson *et al.* and Senthivinayagam *et al.* found that deletion of
321 PANX1 in either white or brown adipose tissue exacerbated diet-induced obesity, specifically by
322 increasing susceptibility to insulin resistance, establishing that PANX1 plays a critical role in
323 glucose homeostasis in the adipose tissue[28,49]. Since cardiomyocytes are among the most energy-
324 demanding cell types requiring high levels of ATP needed for contraction, we examined the role
325 for PANX1 in control of cardiomyocyte metabolism. We demonstrate that PANX1 deletion induces
326 a metabolic shift in the cardiomyocyte by priming the cardiomyocyte toward a glycolytic state at
327 baseline. Consequently, PANX1-deficient cardiomyocytes are less responsive to stress induced by
328 beta-adrenergic receptor activation. We found a significant increase in *Slc2a4* expression in
329 isolated primary murine cardiomyocytes of Panx1^{MyHC6} mice, which is matched by increased
330 glucose uptake and glycolytic rate in PANX1 knock-down H9c2 myoblasts *in vitro*[14]. This glycolytic
331 phenotype has previously been observed in fetal cardiomyocytes and is associated with increased
332 proliferative capacity[11,14]. Furthermore, increased glucose availability and glycolytic rate in
333 unstressed situations leads to better outcomes and is associated with increased regenerative
334 capacity after ischemic/ reperfusion injury[15,60].

335 RNA-Sequencing of isolated cardiomyocytes from Panx1^{MyHC6} and Panx1^{flfl} mice with non-
336 ischemic heart failure revealed significantly decreased expression of genes associated with

337 immune system function. Previous work established that PANX1 deletion in endothelial cells
338 decreases the immune cell recruitment to the myocardium after a myocardial infarction, without
339 further specifying a particular immune cell population[35]. We find that deletion of PANX1 in
340 cardiomyocytes decreases overall immune cell recruitment, which was driven specifically by a
341 significant decrease of neutrophils. Immune cell recruitment to the myocardium has been shown
342 to exacerbate cardiomyocyte damage and impairment of myocardial function[7,61]. Therefore, the
343 decrease in immune cells in the myocardium of mice with PANX1-deficient cardiomyocytes
344 suggests that PANX1 may serve to propagate or initiate the sterile immune response in the
345 myocardium during times of chronic cardiac stress[22]. The changes in gene expression reveal an
346 overall decreased chronic inflammatory state of the myocardium in Panx1^{MyHC6} mice after
347 isoproterenol induced heart failure.

348 While our observations of neutrophil recruitment by PANX1 are in the context of
349 isoproterenol-induced non-ischemic heart failure, PANX1 activation in cardiomyocytes may also
350 be important in ischemic heart failure or after ischemia-reperfusion injury. Future investigations
351 will elucidate if the effects on neutrophil infiltration attributed to cardiomyocyte-specific deletion
352 of PANX1 vary by injury type, which will provide opportunities to develop therapies that are
353 specific to the type of cardiac injury.

354 ATP is known to serve as recruitment or "find me" signal for immune cells during
355 inflammation[62,63] and apoptosis[24,25]. While we do not identify the responsible receptors on
356 neutrophils, our RNA sequencing data demonstrate that expression of key purinergic receptors,
357 namely P2X1, P2Y1, P2Y14, and ADORA2A, is decreased in the whole heart tissue of Panx1^{MyHC6}
358 mice during isoproterenol-induced heart failure. Of these P2Y1, P2Y14, and ADORA2A can be

359 associated with decreased neutrophil recruitment[64]. Moreover, we cannot rule out other
360 purinergic molecules that could be reseased through PANX1 potentially driving the neutrophil
361 recruitment. P2Y1 and ADORA2A bind ADP and adenosine, respectively, which could be
362 generated from local exonucleases acting on the ATP released via PANX1 or could be released
363 from PANX1 itself. Additionally, P2Y14 on neutrophils binds UDP-glucose[65], which can be released
364 through PANX1[25,64]. Therefore, a combination of signaling molecules released by PANX1, including
365 ATP and UDP-glucose, may be necessary for the infiltration of neutrophils into the myocardium
366 during non-ischemic heart failure.

367 Historically, treatment of heart failure in patients has focused on therapies which treat the
368 symptoms of the disease, such as edema and dyspnea, rather than directly targeting cardiac
369 function or preventing functional decline of the cardiac muscle. Previously, clinical trials have
370 identified that spironolactone, a mineralocorticoid receptor antagonist (MRA) and PANX1 blocker,
371 improves patient outcomes in both all-cause mortality and sudden cardiac death in patients with
372 established heart failure over a placebo[33,66,67]. However, it is is not completely clear why this
373 therapy is more beneficial than others which also lower blood pressure. Based on our findings we
374 speculate that this can be explained by the additional action of spironolactone as a PANX1
375 channel blocker. Systemic PANX1 channel blockade may improve patient outcomes by preventing
376 immune cell recruitment, as has been shown in multiple mouse models[24,35,53]. Furthermore,
377 modulating cardiomyocyte metabolism to increase glucose uptake may prevent an energy
378 imbalance which is thought to be a driving factor in the functional decline of cardiac muscle.

379 Taken together our study illustrates how PANX1 deletion in cardiomyocytes protects
380 against the progression of non-ischemic heart failure. We demonstrate that PANX1 channel

381 opening can be induced by beta-adrenergic receptor stimulation in cardiomyocytes.
382 Cardiomyocyte-specific deletion in mice (Panx1^{MyHC6}) impacts their cardiac glycolytic metabolism,
383 which we attribute to a higher expression of *Slc2a4* and increased glucose uptake. Panx1^{MyHC6}
384 mice are protected from isoproterenol-induced non-ischemic heart failure and cardiac
385 hypertrophy, which we demonstrate to be at least in part due to a decrease in neutrophil
386 recruitment. Our findings identify PANX1 in cardiomyocytes as a therapeutic target to prevent
387 severe cardiac tissue damage in non-ischemic heart failure, which may also be relevant for
388 developing therapies targeted at PANX1 for other forms of heart failure such as HFpEF.
389

390 **Methods**

391

392 **Animals:** Cardiomyocyte-specific Panx1-deficient mice were generated by crossing *Panx1*$^{loxP/loxP}$

393 (Panx1$^{fl/fl}$) mice[42] with B6.FVB-Tg(Myh6-cre)2182Mds/J (MyHC6-Cre)[68] (strain #011038) obtained

394 from the Jackson Laboratory. For breeding purposes, mice hemizygous for the MyHC6 Cre were

395 cross with Panx1$^{fl/fl}$ mice to give littermate mice of Panx1$^{loxP/loxP}$ MyHC6$^{wt/wt}$ (Panx1$^{fl/fl)}$ and

396 Panx1$^{loxP/loxP}$ MyHC6 $^{Cre/wt}$ (Panx1^{MyHC6}). All animals were maintained at the University of Virginia

397 Center for Comparative Medicine in a pathogen-free vivarium facility. Mice were maintained on

398 a 12-hour light/dark cycle and provided ad libitum access to standard rodent chow (Teklad 7912)

399 and water. All experiments performed were approved by the University of Virginia Animal Care

400 and Use Committee (protocol #3444). All experiments were performed using age-matched

401 littermate controls. Genotyping was performed via PCR from tail clip biopsies after proteinase K

402 digestion in DirectPCR tail lysis buffer (Viagen Biotech 102-T). PCR of genomic DNA was

403 performed using Apex Taq Master Mix and allele-specific primers as previously described[69].

404 **Isoproterenol induction of heart failure:** 8–10-week-old male mice were treated daily with

405 isoproterenol or saline vehicle for 14 days to induce heart failure as previously described.

406 Isoproterenol (medchem: HYB0468) was freshly prepared daily in sterile saline prior to injection

407 (15 mg/kg/day) and administered by intraperitoneal injection. Mice were weighed daily to

408 monitor for excessive weight loss and appropriate dose administration.

409 **Isoproterenol progression of heart failure:** For longer-term administration of isoproterenol,

410 osmotic pumps (Alzet 2004) were filled with isoproterenol in sterile saline plus 0.02% acetic acid

411 and mice were weighed prior to implantation to administer 15mg/kg/day according to pump rate

412 specifications. Pumps were equilibrated overnight in sterile saline prior to implantation. 8–10-

413 week-old male mice were anesthetized using isoflurane and implantation sites were exposed after
414 hair removal with Nair hair removal lotion with aloe and lanolin. Mice were administered
415 bupivicane analgesic and sites were sterilized with three washes of betadine and ethanol wipes.
416 Pumps were implanted in a subcutaneous pocket on the back of the mouse and surgical clips
417 were placed for wound closure. Mice were placed on a heating-pad and isoflurane anesthesia
418 was maintained for the length of the procedure. Surgical clips were removed 10-14 days after
419 placement.

420 **Immunofluorescence staining:** Hearts were harvested and fixed for 4 hours in 10% zinc-buffered
421 formalin prior to fixation in 50% ethanol. Tissues were paraffin embedded and cryosectioned to
422 7µm thickness and mounted. Slides were deparaffinized. Briefly, sections were submerged in
423 Histo-Clear (Electron Microscopy Sciences 64110-01) (3x10 minutes), 100% ethanol (2x3
424 minutes), 95% ethanol (2x3 minutes), 70% ethanol (1x3 minutes), and PBS (1x5 minutes). Antigen
425 retrieval was performed using citrate-based solution (Vector Laboratories H-330) where slides
426 were submerged in antigen retrieval solution and heated to boiling for 20 minutes, slides were
427 then cooled for 10 minutes at room temperature and 10 minutes at $4^{\circ C}$. Tissue sections were then
428 blocked for 1 hour in antibody blocking buffer (0.2% TritonX, 1mL donkey serum) at room
429 temperature. Antibody blocking buffer was removed and replaced with antibody blocking buffer
430 containing primary antibody (1:100) overnight at $4^{\circ C}$. Sections were then washed (3xPBS for 5
431 minutes) and incubated in antibody blocking buffer containing secondary antibody (1:500) for 1
432 hour at room temperature protected from light. Sections were washed (3xPBS) and
433 counterstained with DAPI (Thermo Fisher Scientific D3571) before mounting. Sections were
434 imaged on an Olympus Fluoview 1000 and are representative images of composite z-stacks.

435 Analysis (thresholding, manual counting, and fluorescence intensity quantification) were
436 performed in ImageJ.

437 **Quantification of Cardiomyocyte cross-sectional area:** Hearts were prepared as indicated in
438 immunofluorescence staining. Sections were stained with cTnnt (1:100 - Abcam ab8295) during
439 primary incubation and DAPI (1:500 - Thermo Fisher D3571) and Wheat-Germ-Agglutinin-Alexa
440 Fluor 647 (5 µg/m – Thermo Fisher W32466) during secondary incubation. Sections were imaged
441 on an Olympus Fluoview 1000 confocal microscope with five images per mouse taken in the left
442 ventricle across two sections. 50 round nucleated cardiomyocytes per mouse were outlined
443 across the images and were analyzed in ImageJ.

444 **Flow cytometry of infiltrating cardiac leukocytes:** Primary infiltrating leukocytes were isolated
445 from cardiac tissue by non-Langendorff perfusion previously described[70]. Briefly, hearts were
446 sequentially perfused with EDTA buffer, perfusion buffer, and digestion buffer containing
447 collagenase until hearts appeared soft. Hearts were then mechanically dissociated with scissors
448 and pipetted up and down. Cells were washed through a 100µm cell strainer to create a single
449 cell suspension. Myocytes were isolated by centrifugation at 120 x g for 5 minutes. Supernatants
450 (containing non-myocyte cells) were transferred to clean tubes and pelleted by centrifugation at
451 300 x g for 5 minutes. Pellets were treated with ACK lysis buffer for 1 minutes and then
452 resuspended in 1mL of FACS buffer (PBS, 2mM EDTA, and 1%BSA). Splenocytes were isolated by
453 grinding through a 100µm cell strainer and washing with PBS containing 2mM EDTA. Samples
454 were then incubated with ACK lysis buffer for 2 minutes and spun at 400 x g for 5 minutes. All
455 samples were then counted and resuspended at 100µL per 100,000 cells in PBS. Cells were
456 stained with LIVE/DEAD Yellow (1:1000) (Thermo Scientific L34967) for 30 minutes on ice. Fc-

457 receptors were then blocked for 15 minutes using FcBlock (BioRad – BUF041A). Cells were
458 pelleted by centrifugation (300 x g,5 minutes) and resuspended in FACS buffer (100µL per 100,000
459 cells) and stained with fluorophore-conjugated antibodies (1:100) for 1 hour on ice. See tables for
460 antibodies included below. Cells were washed in PBS (x3) after staining. Flow cytometry collection
461 and deconvolution was performed on an Cytek Northern Lights 3 laser Spectral Flow Cytometer.
462 Automatic deconvolution was performed using single stains generated from splenocytes. Gating
463 and post-hoc analysis was performed with FCS-Express 7.18. Representative gating is presented
464 for all flow cytometry experiments in supplemental figures.

465 **RNA-Sequencing:** Hearts of mice were removed after whole body perfusion with 10mL of PBS,
466 weighed, and snap frozen at -80^{C} prior to analysis. For some experiments, isolated
467 cardiomyocytes were suspended in 1mL of TRIzol™ (Invitrogen) and stored at -80^{oC} for further
468 analysis[70]. After chloroform incubation and centrifugation per manufacture instructions RNA-
469 containing phase was diluted with 70% ethanol 1:1 and RNA isolation was performed using
470 RNeasy Mini Kit (Qiagen). For tissues, Total RNA was isolated using RNeasy Mini Kit (Qiagen) after
471 lysis in RLT buffer with bead homogenization. Total RNA quantity and quality were then assessed
472 on a NanoDrop 2000 spectrophotometer (Thermo Fisher Scientific). Library preparation including
473 quality metrics, sequencing, and clustering were performed by Novogene (Sacramento, CA).
474 Sample integrity was assessed prior to library preparation using the Bioanalyzer 2110 system with
475 an RNA Nano 6000 Assay Kit (Agilent Technologies). One hundred fifty-base paired-end
476 sequencing was performed using an Illumina NovaSeq platform according to manufacture
477 instructions. Fastq files were processed using in-house perl scripts from Novogene to obtain clean
478 reads. Clean reads were aligned to the mouse reference genome using Hisat2 v2.0.5.

479 FeatureCounts was used to calculate read numbers for each gene and fragments of per kilobase
480 of transcript sequence per millions base pairs sequenced (FPKM) were calculated. Differential
481 expression analysis was performed using DESeq2. Differentially expressed genes (DEG) were
482 assigned by criteria of P-value adjusted < 0.05 (-Log(p-value) > 1.3). KEGG pathway analysis and
483 Gene Ontology pathway analysis was performed on DEG using clusterProfiler.

484 **Echocardiography:** 8–16-week-old male mice were anesthetized using isoflurane. The chest was
485 exposed after hair removal and a four-lead electrocardiogram (ECG) was collected during the
486 procedure. Images were collected using a VevoView 1100 system. Images were collected in the
487 long-axis (B-mode) and short axis (M-mode) on mice serially throughout the experimental period.
488 Serial collection began prior to disease induction and occurred every two-weeks during disease
489 progression. Images were analyzed using Vevo Lab. Left-ventricle (LV) end-diastolic, end-systolic
490 volume, and wall thickness were assessed, and ejection fraction calculated.

491 **Blood Pressure Assessments using Radiotelemetry:** Blood pressure was measured using
492 telemetry equipment (Data Sciences International, DSI) as previously described[27]. Mice were
493 surgically implanted with radiotelemetry units (PA-C10 or HD-X10). Briefly, while under
494 isoflurane anesthesia, the catheter of a radiotelemetry unit was placed in the left carotid artery
495 and positioned such that the probe reached the aortic arch. The radio-transmitter was placed in
496 a subcutaneous pouch at the right flank. Buprenorphine was used as an analgesic. Mice were
497 allowed to recover for seven days prior to the initiation of recordings. Baseline blood pressure
498 measurements, including systolic pressure, diastolic pressure, mean arterial pressure (MAP) and
499 heart rate, were recorded every minute for a continuous period of 5 days using Dataquest A.R.T.
500 20 software (DSI). Diurnal (inactive period) MAP was measured during animal's light cycle (6:00

501 a.m. to 5:59 p.m.) and nocturnal (active period) MAP was measured during the animal's dark
502 cycle (6:00 p.m. to 5:59 a.m.).
503 **Antibodies:** Antibodies used in these studies were rabbit monoclonal anti-Panx1 (Cell Signaling -
504 #91137), rabbit monoclonal anti-CCR2 (Abcam – ab273050), rat monoclonal anti-Ly6g (R&D
505 Systems – MAB1037), mouse monoclonal anti-cardiac troponin T (Abcam – ab8295), and wheat
506 germ agglutinin (Invitrogen – W32466). Flow cytometry antibody used include CD45 rat anti-
507 mouse APC eFluor 780 (Invitrogen - 47-0451-80), CD11b rat anti-mouse FITC (Invitrogen - 11-
508 0112-82), CD163 rat anti-mouse PE (Invitrogen - 12-1631-80), CD86 rat anti-mouse SuperBright
509 436 (Invitrogen - 62-0869-41), LIVE/DEAD Yellow Cell Stain for 405 (L34967), Ly6g rat anti-mouse
510 PE-Cyanine5 (Invitrogen - 15-9668-80), F4/80 anti-mouse APC (eBioscience 17-4801-82), CD64
511 anti mouse PerCP-710 (Invitrogen – 46-0641-80), CD24 anti mouse PE-Cyanine7 (Invitrogen 25-
512 0242-82).
513 **Cell culture:** H9c2 rat myoblasts were obtained from ATTC and maintained in high-glucose DMEM
514 supplemented with 10% heat-inactivated FBS, 15 mM sodium bicarbonate (Glibco), 1mM sodium
515 pyruvate (Glibco), and 1% Pen-Strep. Cells were passaged when they reached 70% confluency on
516 tissue culture (TC) treated dishes using 0.25% trypsin (Glibco).
517 **siRNA-Mediated Knock-Down of Panx1:** H9c2 cells in 12 or 24 well TC treated plates or 10cm TC
518 treated dishes were washed in sterile PBS and then incubated with OptiMEM (Glibco). Cells were
519 treated with RNAiMax Lipofectamine and siRNA against Panx1 or negative control silencer #1
520 (Ambion - 197003) per the manufacturer's instructions. Experiments were performed 72 hours
521 after transfection with the siRNA.
522

523 **RNA isolation and quantitative reverse transcription PCR:** RNA was isolated from approximately
524 75,000 H9c2 rat myoblasts or isolated cardiomyocytes from one mouse heart and lysed in RLT
525 lysis buffer. RNA was isolated using the RNeasy Mini Kit (QIAGEN) according to the manufacturer's
526 instructions. RNA was quantified using a NanoDrop spectrophotometer (Thermo Fisher
527 Scientific), and complementary DNA (cDNA) libraries were generated using the iScript cDNA
528 Synthesis Kit (Bio-Rad). Quantitative reverse transcription PCR was performed using TaqManFast
529 Advanced Master Mix (Thermo Fisher Scientific) and TaqMan primers (mouse *Panx1* mm0045091
530 – Invitrogen) (Rat *Panx1* Rn01447976_m1 – Thermo Fisher Scientific) for genes of interest on a
531 CFX Connect real-time PCR instrument (Bio-Rad). Relative gene expression was determined using
532 *18S* (4333760 – Thermo Fisher Scientific) or *Hprt* (mm01545399 – Invitrogen) as a housekeeping
533 gene.
534 **ATP release measurements:** H9c2 cells were plated at 80,000 cells per well in a 48 well dish and
535 put in serum free media overnight prior to experimental treatment. Cells were incubated with
536 Panx1 inhibitors (spironolactone 50 µM in serum free media) or vehicle control for 1 hour prior
537 to stimulation. ARL (Tocris 1283) (300 µM) was added for 30 minutes prior to stimulation. Cells
538 were then stimulated with vehicle (PBS), isoproterenol (2 or 20 µM in sterile PBS), or
539 phenylephrine positive control (10 µM) for 15 minutes. One-third of the media in the well was
540 carefully collected with care taken to not bump cells in the bottom of the well and placed on ice.
541 ATP concentrations were assessed by CellTiterGlo (Promega G7571) and compared to standard
542 curve prepared by combining serum free H9c2 media with ATP disodium salt (Tocris 3245).
543 **Dye Uptake Assay:** H9c2 cells were plated at 1000,000 cells per well in a 12 well dish and
544 incubated with Panx1 inhibitors (spironolactone 50 µM, carbenoxolone 50 µM, or probenecid

545 1mM) or vehicle control for 1 hour prior to stimulation. Cells were stimulated with vehicle (PBS),
546 isoproterenol (2 or 20 µM in sterile PBS), or phenylephrine positive control (10 µM) for 1 hour at
547 the same time as Yo-Pro-1 dye (Thermo Fisher Scientific Y3603) (1µM) was added to the media.
548 Media was removed and cells were washed prior to detachment with trypsin (0.25%). Cells were
549 spun at 400 x g for 5 minutes and resuspended in PBS with LIVE/DEAD Yellow (1:1000) for 30
550 minutes. Cells were pelleted and washed in Annexin V binding buffer three times and then
551 resuspended in Annexin V AlexaFluor 568 (Thermo Fisher Scientific A13202) (1:500) (AV) for 10
552 minutes. Cells were washed and resuspended in FACS buffer as described above. Cells were
553 analyzed by flow cytometry on an Attune NxT. Single stain controls were performed using H9c2
554 cells for initial intensity. FMO were collected and used for deconvolution prior to gating. Cells
555 were gated for LIVE/DEAD Yellow and AV negative and the percentage of cells positive for Yo-Pro-
556 1 was assessed as compared to vehicle stimulation.
557 **Glycolytic Stress Test:** After treatment with control or Panx1-targeting siRNA as described above,
558 H9c2 rat myoblasts were plated (40,000 cells per well) in complete medium in XFe96 cell culture
559 microplate and allowed to settle for one hour at room temperature before overnight culture. The
560 following day cells were treated with ISO (20µM) for 1 hour in complete medium. Immediately
561 prior to the assay the media was changed to glycolytic stress test medium (Sigma Aldrich D5030)
562 supplemented with 143 mM NaCl and 2mM L-glutamine (Gibco 25030 – 081). Glycolytic activity
563 was assessed by measurement of extracellular acidification rate on a Seahorse XFe96 instrument
564 (Agilent Technologies). The rate of pH change was measured every 13 minutes for a 3-minute
565 interval before sequential challenge with 1) 20mM glucose (Sigma Aldrich D9434), 2) 1 µM
566 oligomycin (Sigma Aldrich 75351), and 3) 80 mM 2-deoxyglucose (Sigma Aldrich D8375). Basal

567 ECAR was measured as post-glucose ECAR minus post 2-DG ECAR, and maximal ECAR was
568 measured as post-oligomycin ECAR minus post-2DG ECAR.
569 **2-NDB Glucose Uptake:** H9c2 rat myoblasts were plated in a black, clear bottom 96 well plate and
570 allowed to adhere overnight in complete media. Cells had been cultured with either control or
571 Panx1 siRNA for 48 hours in OptiMem media prior to plating. The following day cells were treated
572 with ISO (20µM) for 1 hour or vehicle control. After stimulation media was removed and replaced
573 with glucose free DMEM as described above in the presence of 2-NDB glucose for 4 hours. The
574 uptake of fluorescent 2-NBDG was assessed according to manufacturer's instructions (Cayman
575 Chemicals - Glucose Uptake Cell-Based Assay Kit) on a Synergy HTX plate reader (BioTek).
576 **CytoTox Cell Death Assay:** H9c2 rat myoblasts were plated in a clear bottom 96 well plate and
577 allowed to adhere overnight in complete phenol red free media. Cells had been cultured with
578 either control or Panx1 siRNA for 48 hours in OptiMem media prior to plating. The following day
579 cells were treated with ISO (2,20µM) or phenylephrine (10 µM) for 15 minutes or vehicle control.
580 After stimulation media was removed and LDH presence in the media was assessed according to
581 manufacturer's instructions (Promega- CytoTox Non-radioactive cytotoxicity assay) on a Synergy
582 HTX plate reader (BioTek).
583 **Serum Creatinine:** Whole blood was collected from mice via cardiac puncture and placed into
584 serum separating tubes (BD Microtainer – 365967) for 30 minutes at room temperature. Serum
585 was separated by centrifugation (1500 x g, 5 minutes) and snap frozen on dry ice. Serum
586 creatinine was measured at 520 nm after addition of sodium picrate according to manufacturer's
587 instructions (Pointe Scientific - Creatinine Reagent Set C75391250) using a known standard
588 (Pointe Scientific C75391250).

589 **Statistics:** Statistical analyses were performed in Prism 9 (GraphPad). The presence of statistical
590 outliers was assessed by a ROUT test (2%), and identified outliers were excluded from analysis.
591 Statistical outliers were identified for data show in Figure 4E, F, which were excluded from
592 analysis. Statistical tests were performed with two-tailed analysis. Comparisons between two
593 groups was conducted by Welch's or Student's t-test, while comparisons between more than two
594 groups were made by one-way analysis of variance or mixed-effects analysis. Sidak's multiple
595 comparisons test was performed as post-hoc analysis where appropriate. Mixed effects analysis
596 was used for paired data with more than two groups. A p-value of less than 0.05 was considered
597 statistically significant. Data are represented as mean ± the standard error of the mean. Image
598 analysis was performed on 3-5 averaged images per mouse across a minimum of two cardiac
599 sections. Data points shown for imaging are representative of the average across a mouse, with
600 each data point representative of individual mice.
601 **Data Availability:** Sequencing data reported in this manuscript are deposited in the NCBI Gene
602 expression Omnibus. All data needed to evaluate the conclusions of this manuscript are present
603 in the manuscript, present in the supplementary figures, or available upon request to the
604 corresponding author. Graphics were prepared using BioRender. Panx1^{MyHC6} mice can be provided
605 by N.L. upon completion of a materials transfer agreement with the University of Virginia School
606 of Medicine. Requests may be submitted to N.L. (nl2q@virginia.edu).
607

608 **References:**

609 1. Tsao, C. W. *et al.* Heart Disease and Stroke Statistics—2023 Update: A Report From the
610 American Heart Association. *Circulation* CIR.0000000000001123 (2023)
611 doi:10.1161/CIR.0000000000001123.
612 2. Schiattarella, G. G. & Hill, J. A. Cardiometabolic HFpEF: Mechanisms and Therapies.
613 *CardioMetabolic Syndr. J.* **1**, 117 (2021).
614 3. Simmonds, S. J., Cuijpers, I., Heymans, S. & Jones, E. A. V. Cellular and Molecular Differences
615 between HFpEF and HFrEF: A Step Ahead in an Improved Pathological Understanding. *Cells*
616 **9**, (2020).
617 4. Berthiaume, J. M. *et al.* Chapter 8 - Pathophysiology of Heart Failure and an Overview of
618 Therapies. in *Cardiovascular Pathology (Fourth Edition)* (eds. Buja, L. M. & Butany, J.) 271–
619 339 (Academic Press, 2016). doi:10.1016/B978-0-12-420219-1.00008-2.
620 5. Chavey, W. E., Hogikyan, R. V., Harrison, R. V. & Nicklas, J. M. Heart Failure Due to Reduced
621 Ejection Fraction: Medical Management. *Am. Fam. Physician* **95**, 13–20 (2017).
622 6. McMurray, J. J. V. & Packer, M. How Should We Sequence the Treatments for Heart Failure
623 and a Reduced Ejection Fraction? A Redefinition of Evidence-Based Medicine. *Circulation*
624 CIRCULATIONAHA.120.052926 (2020) doi:10.1161/CIRCULATIONAHA.120.052926.
625 7. Zhang, Y., Bauersachs, J. & Langer, H. F. Immune mechanisms in heart failure. *Eur. J. Heart*
626 *Fail.* **19**, 1379–1389 (2017).
627 8. Travers, J. G., Tharp, C. A., Rubino, M. & McKinsey, T. A. Therapeutic targets for cardiac
628 fibrosis: from old school to next-gen. *J. Clin. Invest.* **132**, e148554 (2022).

9. Fearnley, C. J., Roderick, H. L. & Bootman, M. D. Calcium Signaling in Cardiac Myocytes. *Cold Spring Harb. Perspect. Biol.* **3**, (2011).
10. Williams, G. S. B., Boyman, L. & Lederer, W. J. Mitochondrial calcium and the regulation of metabolism in the heart. *J. Mol. Cell. Cardiol.* **78**, 35–45 (2015).
11. Lopaschuk, G. D. & Jaswal, J. S. Energy Metabolic Phenotype of the Cardiomyocyte During Development, Differentiation, and Postnatal Maturation. *J. Cardiovasc. Pharmacol.* **56**, 130–140 (2010).
12. Neubauer, S. The Failing Heart — An Engine Out of Fuel. *N. Engl. J. Med.* **356**, 1140–1151 (2007).
13. Fragasso, G. Deranged Cardiac Metabolism and the Pathogenesis of Heart Failure. *Card. Fail. Rev.* **2**, 8–13 (2016).
14. Razeghi, P. *et al.* Metabolic Gene Expression in Fetal and Failing Human Heart. *Circulation* **104**, 2923–2931 (2001).
15. Li, X. *et al.* Inhibition of fatty acid oxidation enables heart regeneration in adult mice. *Nature* **622**, 619–626 (2023).
16. Dolmatova, E. *et al.* Cardiomyocyte ATP release through pannexin 1 aids in early fibroblast activation. *Am. J. Physiol. - Heart Circ. Physiol.* **303**, H1208–H1218 (2012).
17. Sager, H. B. *et al.* Proliferation and Recruitment Contribute to Myocardial Macrophage Expansion in Chronic Heart Failure. *Circ. Res.* **119**, 853–864 (2016).
18. Benjamin, I. J. *et al.* Isoproterenol-induced myocardial fibrosis in relation to myocyte necrosis. *Circ. Res.* **65**, 657–670 (1989).

650 19. Revelo, X. *et al.* Cardiac Resident Macrophages Prevent Fibrosis and Stimulate Angiogenesis.
651 *Circ. Res.* CIRCRESAHA.121.319737 (2021) doi:10.1161/CIRCRESAHA.121.319737.
652 20. Blanton, R. M., Carrillo-Salinas, F. J. & Alcaide, P. T-cell recruitment to the heart: friendly
653 guests or unwelcome visitors? *Am. J. Physiol.-Heart Circ. Physiol.* **317**, H124–H140 (2019).
654 21. Lavine, K. J. *et al.* The Macrophage in Cardiac Homeostasis and Disease. *J. Am. Coll. Cardiol.*
655 **72**, 2213–2230 (2018).
656 22. Frieler, R. A. & Mortensen, R. M. Immune Cell and Other Non-Cardiomyocyte Regulation of
657 Cardiac Hypertrophy and Remodeling. *Circulation* **131**, 1019–1030 (2015).
658 23. Hartman, M. H. T., Groot, H. E., Leach, I. M., Karper, J. C. & van der Harst, P. Translational
659 overview of cytokine inhibition in acute myocardial infarction and chronic heart failure.
660 *Trends Cardiovasc. Med.* **28**, 369–379 (2018).
661 24. Chekeni, F. B. *et al.* Pannexin 1 channels mediate 'find-me' signal release and membrane
662 permeability during apoptosis. *Nature* **467**, 863–867 (2010).
663 25. Medina, C. B. *et al.* Metabolites released from apoptotic cells act as tissue messengers.
664 *Nature* **580**, 130–135 (2020).
665 26. Narahari, A. K. *et al.* ATP and large signaling metabolites flux through caspase-activated
666 Pannexin 1 channels. *eLife* **10**, e64787 (2021).
667 27. Billaud, M. *et al.* A molecular signature in the pannexin1 intracellular loop confers channel
668 activation by the α1 adrenoreceptor in smooth muscle cells. *Sci. Signal.* **8**, ra17–ra17 (2015).
669 28. Senthivinayagam, S. *et al.* Adaptive thermogenesis in brown adipose tissue involves
670 activation of pannexin-1 channels. *Mol. Metab.* **44**, 101130 (2021).

671 29. Zhang, Y. *et al.* Role of cAMP in Cardiomyocyte Viability: Beneficial or Detrimental? *Circ. Res.*
672 **133**, 902–923 (2023).
673 30. Chiu, Y.-H. *et al.* A quantized mechanism for activation of pannexin channels. *Nat. Commun.*
674 **8**, 14324 (2017).
675 31. Michalski, K. & Kawate, T. Carbenoxolone inhibits Pannexin1 channels through interactions
676 in the first extracellular loop. *J. Gen. Physiol.* **147**, 165–174 (2016).
677 32. Silverman, W., Locovei, S. & Dahl, G. Probenecid, a gout remedy, inhibits pannexin 1
678 channels. *Am. J. Physiol. Cell Physiol.* **295**, C761-767 (2008).
679 33. Good, M. E. *et al.* Pannexin 1 Channels as an Unexpected New Target of the Anti-
680 Hypertensive Drug Spironolactone. *Circ. Res.* **122**, 606–615 (2018).
681 34. Rusiecka, O. M. *et al.* Mitochondrial pannexin1 controls cardiac sensitivity to
682 ischaemia/reperfusion injury. *Cardiovasc. Res.* **119**, 2342–2354 (2023).
683 35. Good Miranda E *et al.* Endothelial Pannexin 1 Regulates Cardiac Response to Myocardial
684 Infarction. *Circ. Res.* **0**,.
685 36. Li, L., He, L., Wu, D., Chen, L. & Jiang, Z. Pannexin-1 channels and their emerging functions in
686 cardiovascular diseases. *Acta Biochim. Biophys. Sin.* **47**, 391–396 (2015).
687 37. Oudit, G. Y. *et al.* Phosphoinositide 3-Kinase γ–Deficient Mice Are Protected From
688 Isoproterenol-Induced Heart Failure. *Circulation* **108**, 2147–2152 (2003).
689 38. Balakumar, P., Singh, A. P. & Singh, M. Rodent models of heart failure. *J. Pharmacol. Toxicol.*
690 *Methods* **56**, 1–10 (2007).
691 39. Yang, Y. *et al.* Apelin-13/APJ induces cardiomyocyte hypertrophy by activating the Pannexin-
692 1/P2X7 axis and FAM134B-dependent reticulophagy. *J. Cell. Physiol.* **237**, 2230–2248 (2022).

693 40. Valentine, C. D. & Haggie, P. M. Confinement of β_1- and β_2-adrenergic receptors in the
694 plasma membrane of cardiomyocyte-like H9c2 cells is mediated by selective interactions
695 with PDZ domain and A-kinase anchoring proteins but not caveolae. *Mol. Biol. Cell* **22**,
696 2970–2982 (2011).
697 41. Branco, A. F. *et al.* Isoproterenol Cytotoxicity is Dependent on the Differentiation State of
698 the Cardiomyoblast H9c2 Cell Line. *Cardiovasc. Toxicol.* **11**, 191–203 (2011).
699 42. Poon, I. K. H. *et al.* Unexpected link between an antibiotic, pannexin channels and
700 apoptosis. *Nature* **507**, 329–334 (2014).
701 43. Heiman, P. *et al.* Mitochondrial dysfunction associated with TANGO2 deficiency. *Sci. Rep.* **12**,
702 3045 (2022).
703 44. Lujan, A. L. *et al.* Defects in lipid homeostasis reflect the function of TANGO2 in phospholipid
704 and neutral lipid metabolism. *eLife* **12**, e85345 (2023).
705 45. Lee, V. R. *et al.* Pannexin 1 regulates adipose stromal cell differentiation and fat
706 accumulation. *Sci. Rep.* **8**, 16166 (2018).
707 46. Sayedyahossein, S. *et al.* Pannexin 1 binds β-catenin to modulate melanoma cell growth and
708 metabolism. *J. Biol. Chem.* **296**, 100478 (2021).
709 47. Jorquera, G. *et al.* High extracellular ATP levels released through pannexin-1 channels
710 mediate inflammation and insulin resistance in skeletal muscle fibres of diet-induced obese
711 mice. *Diabetologia* **64**, 1389–1401 (2021).
712 48. Banuelos, A. *et al.* Pannexin-1 channels promotes CD8+ T cell effector and memory
713 responses through distinct metabolic pathways. *J. Immunol.* **210**, 226.15-226.15 (2023).

714 49. Adamson, S. E. *et al.* Pannexin 1 is required for full activation of insulin-stimulated glucose
715 uptake in adipocytes. *Mol. Metab.* **4**, 610–618 (2015).
716 50. Sun, J. *et al.* Human Relaxin-2 Fusion Protein Treatment Prevents and Reverses
717 Isoproterenol-Induced Hypertrophy and Fibrosis in Mouse Heart. *J. Am. Heart Assoc.* **8**,
718 e013465 (2019).
719 51. Von Hundelshausen, P. & Weber, C. Platelets as Immune Cells: Bridging Inflammation and
720 Cardiovascular Disease. *Circ. Res.* **100**, 27–40 (2007).
721 52. Filiberto, A. C. *et al.* Endothelial pannexin-1 channels modulate macrophage and smooth
722 muscle cell activation in abdominal aortic aneurysm formation. *Nat. Commun.* **13**, 1521
723 (2022).
724 53. Metz, L. M. *et al.* Platelet pannexin-1 channels modulate neutrophil activation and migration
725 but not the progression of abdominal aortic aneurysm. *Front. Mol. Biosci.* **10**, 1111108
726 (2023).
727 54. Bisht, K. *et al.* Capillary-associated microglia regulate vascular structure and function
728 through PANX1-P2RY12 coupling in mice. *Nat. Commun.* **12**, 5289 (2021).
729 55. Burnstock, G. & Boeynaems, J.-M. Purinergic signalling and immune cells. *Purinergic Signal.*
730 **10**, 529–564 (2014).
731 56. Lohman, A. W. *et al.* Pannexin 1 channels regulate leukocyte emigration through the venous
732 endothelium during acute inflammation. *Nat. Commun.* **6**, 7965 (2015).
733 57. Burnstock, G. Purinergic Signalling: Therapeutic Developments. *Front. Pharmacol.* **8**, 661
734 (2017).

735 58. Birkenfeld, A. L., Jordan, J., Dworak, M., Merkel, T. & Burnstock, G. Myocardial metabolism
736 in heart failure: Purinergic signalling and other metabolic concepts. *Pharmacol. Ther.* **194**,
737 132–144 (2019).
738 59. Burnstock, G. & Pelleg, A. Cardiac purinergic signalling in health and disease. *Purinergic*
739 *Signal.* **11**, 1–46 (2015).
740 60. Tran Diem H. & Wang Zhao V. Glucose Metabolism in Cardiac Hypertrophy and Heart
741 Failure. *J. Am. Heart Assoc.* **8**, e012673 (2019).
742 61. Martini Elisa *et al.* Single-Cell Sequencing of Mouse Heart Immune Infiltrate in Pressure
743 Overload–Driven Heart Failure Reveals Extent of Immune Activation. *Circulation* **140**, 2089–
744 2107 (2019).
745 62. Li, X. *et al.* Systemic Adenosine Triphosphate Impairs Neutrophil Chemotaxis and Host
746 Defense in Sepsis. *Crit. Care Med.* **45**, e97–e104 (2017).
747 63. Bao, Y., Chen, Y., Ledderose, C., Li, L. & Junger, W. G. Pannexin 1 Channels Link
748 Chemoattractant Receptor Signaling to Local Excitation and Global Inhibition Responses at
749 the Front and Back of Polarized Neutrophils. *J. Biol. Chem.* **288**, 22650–22657 (2013).
750 64. Wang, X. & Chen, D. Purinergic Regulation of Neutrophil Function. *Front. Immunol.* **9**, 399
751 (2018).
752 65. Sesma, J. I. *et al.* The UDP-sugar-sensing $P2Y_{14}$ receptor promotes Rho-mediated signaling
753 and chemotaxis in human neutrophils. *Am. J. Physiol.-Cell Physiol.* **303**, C490–C498 (2012).
754 66. Pitt, B. *et al.* The Effect of Spironolactone on Morbidity and Mortality in Patients with Severe
755 Heart Failure. *N. Engl. J. Med.* **341**, 709–717 (1999).

67. Ferreira, J. P. *et al.* Proteomic and Mechanistic Analysis of Spironolactone in Patients at Risk for HF. *JACC Heart Fail.* (2021) doi:10.1016/j.jchf.2020.11.010.

68. Agah, R. *et al.* Gene recombination in postmitotic cells. Targeted expression of Cre recombinase provokes cardiac-restricted, site-specific rearrangement in adult ventricular muscle in vivo. https://www.jci.org/articles/view/119509/pdf (1997) doi:10.1172/JCI119509.

69. Poon, I. K. H. *et al.* Unexpected link between an antibiotic, pannexin channels and apoptosis. *Nature* **507**, 329–334 (2014).

70. Ackers-Johnson Matthew *et al.* A Simplified, Langendorff-Free Method for Concomitant Isolation of Viable Cardiac Myocytes and Nonmyocytes From the Adult Mouse Heart. *Circ. Res.* **119**, 909–920 (2016).

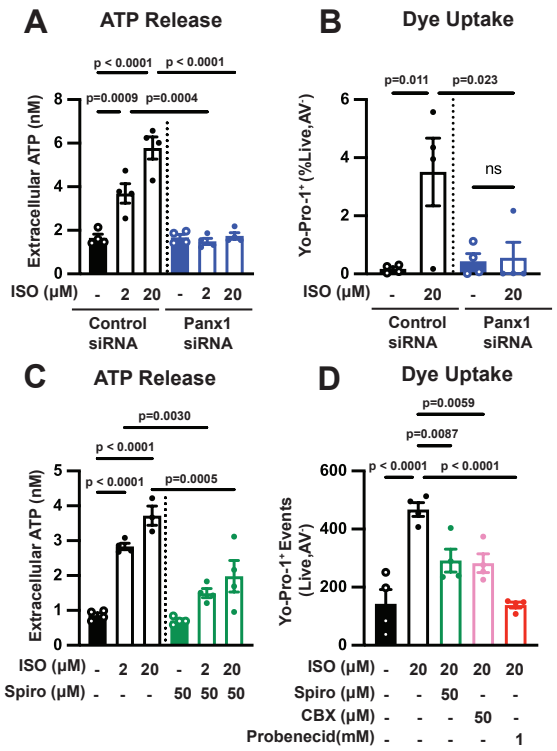

Figure 1: Beta-adrenergic receptor stimulation activates Pannexin 1 channels in cardiomyocytes *in vitro*

A) H9c2 were transfected with either control or Panx1-targeting siRNA for 72 hours and extracellular concentration of ATP was measured after 15 minutes of stimulation with isoproterenol (ISO) (2 and 20μM) or vehicle control. (N=4)

B) Flow cytometric analysis of Yo-Pro-1 dye uptake by control of Panx1-targeting siRNA treated H9c2 cells after stimulation with 20μM ISO (gated for live, annexin V^- cells). (N=4)

C) H9c2 cells were pretreated with spironolactone (50μM) or vehicle control and extracellular ATP levels were measured after 15 minutes of stimulation with isoproterenol (ISO) (2 and 20μM). (N=4)

D) Yo-Pro-1 dye uptake by H9c2 cells treated with isoproterenol (20µM) after pretreatment with spironolactone, carbenoxolone (CBX), or probenecid at the listed concentrations. (N=4)

Data are represented as mean ± standard error of the mean (SEM). Data shown are representatives of 2 independent experiments. Significance determined using One-way ANOVA (A, B, C, D) with Sidak's multiple comparison test for post-hoc analysis for comparisons between individual groups. ns = not significant See also S1 in reference to figure 1.

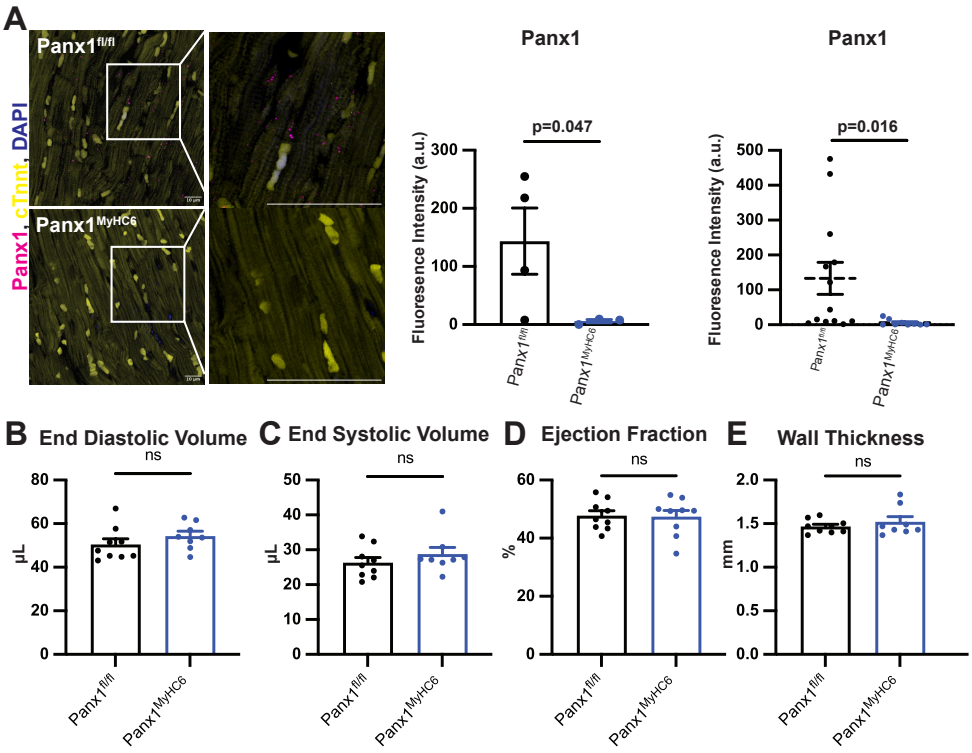

Figure 2: Generation and Characterization of a novel Pannexin 1 cardiomyocyte specific deletion mouse

A) Confocal micrographs of cardiomyocyte-rich whole heart sections from 12-week-old male Panx1$^{fl/fl}$ and Panx1^{MyHC6} mice. Knockout of PANX1 in cardiomyocytes was assessed using immunofluorescent staining. Cardiac troponin T (cTnnt) was used to stain cardiomyocytes; DAPI was used as a nuclear stain. Left, representative micrographs with insets showing PANX1 punctate; middle, average Panx1 fluorescence intensity for individual mice; right, fluorescence intensities for individual micrographs showing demonstrating of PANX1 signal. (Panx1$^{fl/fl}$ N=4 mice N=13 images, Panx1^{MyHC6} N=3 mice N=9 images, 3-5 images per mouse averaged).

B) End-diastolic volume C) End-systolic volume D) Ejection fraction and E) Wall thickness were measured in anesthetized 8- to 10-week-old male Panx1$^{fl/fl}$ and Panx1^{MyHC6} mice using *in vivo* 2D-echocardiography. (Panx1$^{fl/fl}$ N= 9 mice, Panx1^{MyHC6} N=8)

Data represented as mean $\pm$ SEM. Significance was determined by Welch's t-test (A-E).

ns = not significant. See also S2 in reference to figure 2.

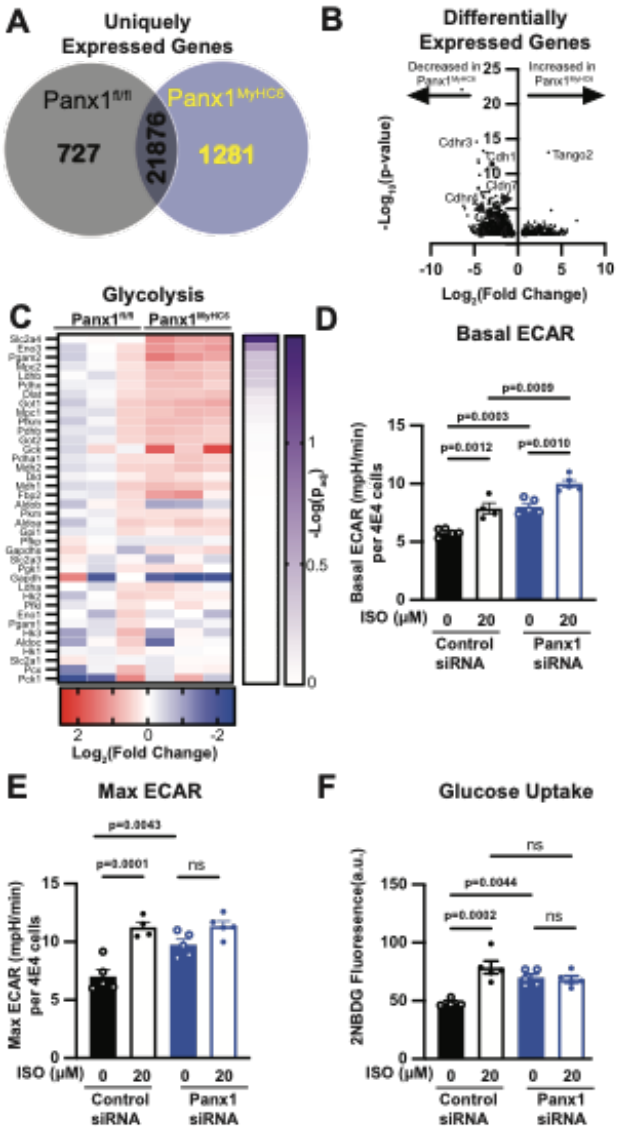

Figure 3: Pannexin 1 deletion shifts cardiomyocyte metabolism from oxidative phosphorylation to glycolysis both *in vivo* and *in vitro*

A) Quantification of uniquely expressed genes from bulk RNA-Sequencing of isolated cardiomyocytes from untreated 12-week-old male $Panx1^{fl/fl}$ and $Panx1^{MyHC6}$ mice.

B) Volcano plot of differentially expressed genes with a cut off of $p < 0.05$. Individual genes are indicated with gene name and arrow.

C) Heatmap showing relative gene expression of glycolysis associated genes from isolated cardiomyocytes of untreated $Panx1^{fl/fl}$ and $Panx1^{MyHC6}$ mice plotted as the Log_2 (fold change) from $Panx1^{fl/fl}$ mouse. Purple heatmap represents -log(p-value) of two-tailed t-tests comparing fold change of $Panx1^{fl/fl}$ and $Panx1^{MyHC6}$. ($Panx1^{fl/fl}$ N=3 mice, $Panx1^{MyHC6}$ N=3 mice)

D) Quantification of Basal extracellular acidification rate (ECAR) and

E) Maximal ECAR of control of Panx1-targeted siRNA treated H9c2 cells after stimulation with either vehicle or ISO (20µM) for 1 hour. (N=5)

F) Glucose uptake as measured by 2NBD-glucose fluorescence intensity of control or Panx1-targeted siRNA treated after 1 hour ISO (20µM) stimulation. (N=4)

Data represented as mean $\pm$ SEM. Significance determined using One-way ANOVA (D, E, F) with Sidak's multiple comparison test for post-hoc analysis for comparisons between individual groups. ns = not significant. See also S3 in reference to figure 3.

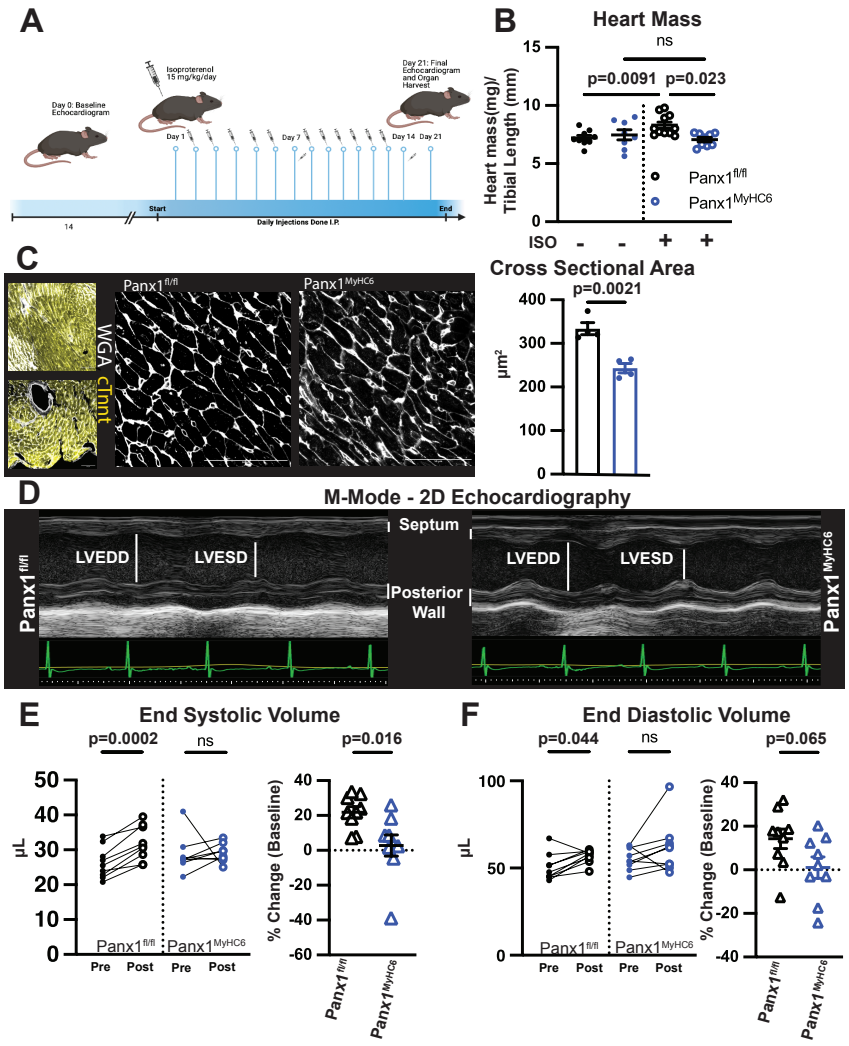

Figure 4: Isoproterenol induced cardiac hypertrophy and dysfunction is abrogated in Panx1^{MyHC6} mice

A) Schematic of experimental model of isoproterenol induced non-ischemic heart failure.

B) Normalized heart mass from 10–12-week-old Panx1$^{fl/fl}$ or Panx1^{MyHC6} mice treated for 14 days with isoproterenol (15 mg/kg/day), or saline control normalized to tibial length. (Saline: Panx1$^{fl/fl}$ N=9, Panx1^{MyHC6} N= 8; Isoproterenol Panx1$^{fl/fl}$ N=11, Panx1^{MyHC6} N= 9)

C) Representative confocal micrographs of wheat germ agglutinin (WGA) staining at 20X (Left) and 60X (Right) from Panx1$^{fl/fl}$ or Panx1^{MyHC6} mice treated with isoproterenol for

14 days. Cardiomyocyte cross sectional area was calculated from WGA. (Panx1$^{fl/fl}$ N=4 mice, Panx1^{MyHC6} N=4, data points represent average of 50 cells per mouse).

D) Representative M-mode images of Panx1$^{fl/fl}$ mice or Panx1^{MyHC6} after 14 days of isoproterenol treatment, visualized by 2D echocardiography.

E) Left, paired analysis of left ventricle end-systolic volume (µL) pre- and post-isoproterenol treatment; right, percent change from baseline after isoproterenol treatment. (Panx1$^{fl/fl}$ N=8, Panx1^{MyHC6} N=9)

F) Left, paired analysis of left ventricle end-diastolic volume (µL) pre- and post-isoproterenol treatment; right, percent change from baseline after isoproterenol treatment. (Panx1$^{fl/fl}$ N=8, Panx1^{MyHC6} N=9)

Data represented as mean $\pm$ SEM. Significance determined using One-way ANOVA (B with Sidak's multiple comparison test for post-hoc analysis for comparisons between individual groups; Student's t-test (C) and Welch's t-test (E, F) was used for comparison between two groups. Significance of paired data was determined using Mixed effects analysis (E, F) with Sidak's multiple comparison test for post-hoc analysis for comparisons between timepoints. ns = not significant. See also S4, S5 in reference to figure 4.

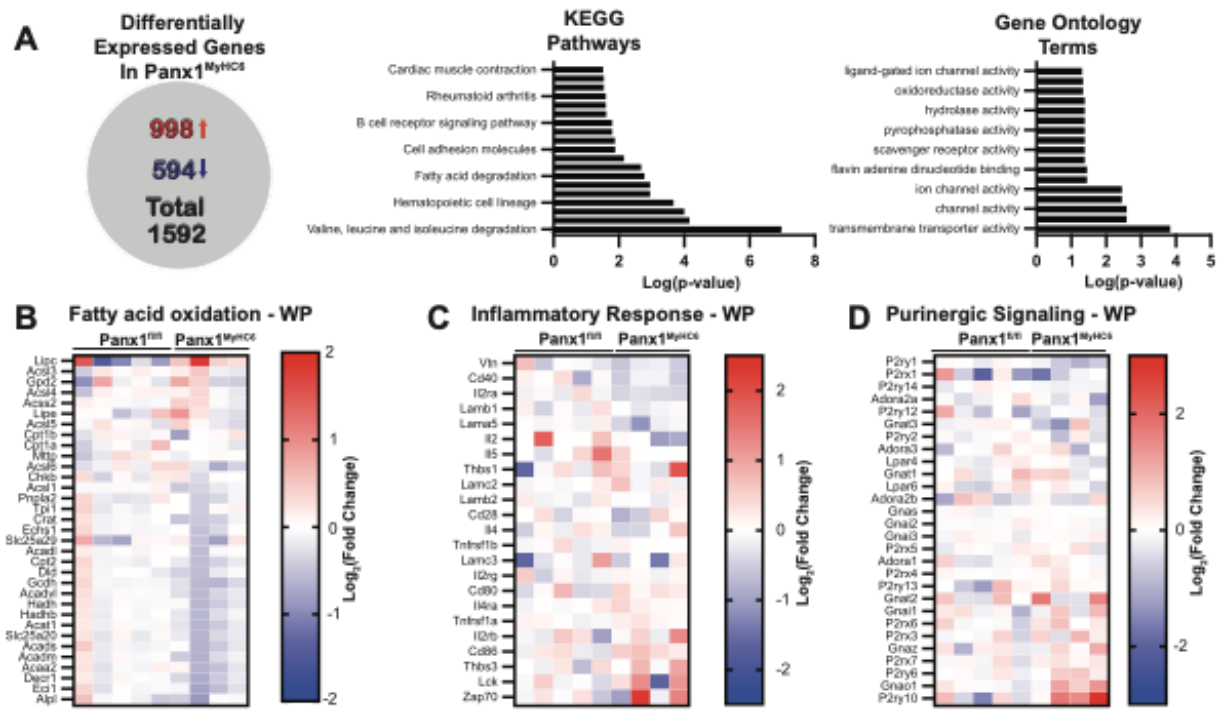

Figure 5: Cardiomyocyte PANX1 knockout leads to transcriptional downregulation of fatty acid metabolism and immune activation pathways during non-ischemic heart failure

A) Quantification of differentially expressed genes identified in bulk RNA-Sequencing between whole hearts of Panx1$^{fl/fl}$ and Panx1^{MyHC6} mice after 14 days of isoproterenol treatment. Differentially expressed gene determined by cut off of $p < 0.05$. Significantly changed, as determined by cut off of $p < 0.05$, KEGG Pathways and Gene Ontology (GO) Terms identified from differentially expressed genes plotted as ordered by -log(p-value).

B) Heatmap demonstrating genes identified in WikiPathways “Inflammatory response”.

C) Heatmap demonstrating genes identified in WikiPathways “Fatty acid oxidation and Fatty acid beta-oxidation”.

D) Heatmap demonstrating genes identified in WikiPathways “Purinergic signaling”. Gradient plotted as Log_2(Fold Change) of $Panx1^{MyHC6}$ compared to $Panx1^{fl/fl}$. ($Panx1^{fl/fl}$ N=5, $Panx1^{MyHC6}$ N=4)

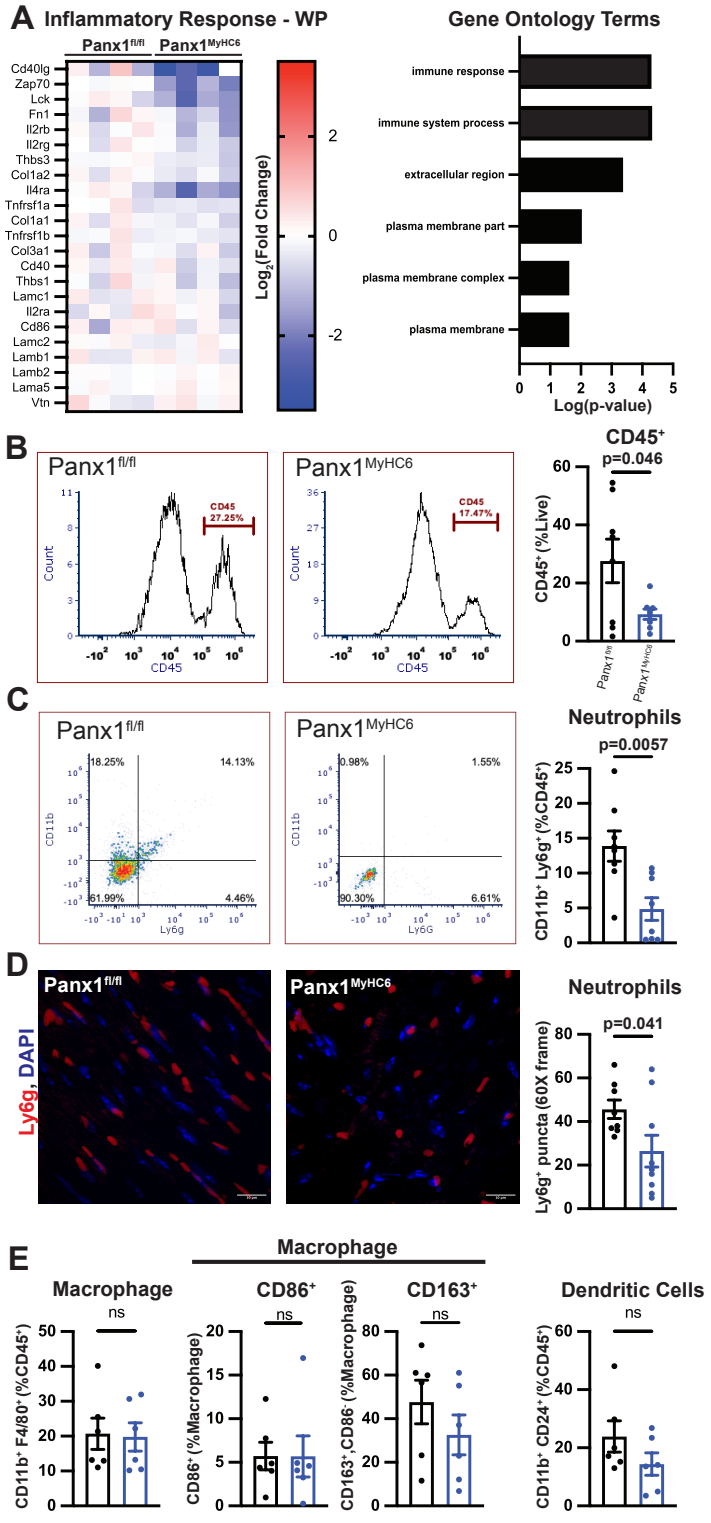

Figure 6: Neutrophil infiltration is significantly blunted in Panx1^{MyHC6} mice during heart failure induced by isoproterenol

A) Heatmap demonstrating genes identified in WikiPathway "Inflammatory response". Gradient plotted as Log_2(Fold Change) of Panx1^{MyHC6} isolated cardiomyocytes after 14-days of isoproterenol treatment compared to Panx1$^{fl/fl}$. Significantly decreased, as determined by cut off of $p < 0.05$, GO terms in Panx1^{MyHC6} cardiomyocytes compared with Panx1$^{fl/fl}$ cardiomyocytes. (Panx1$^{fl/fl}$ N=4, Panx1^{MyHC6} N=4 mice).

B) Flow cytometric analysis of CD45$^+$ cells as a percentage of total live cells isolated from Panx1$^{fl/fl}$ and Panx1^{MyHC6} hearts after 14-days of isoproterenol treatment as identified. Representative histograms of the CD45 populations from live parent gate. (Panx1$^{fl/fl}$ N=8, Panx1^{MyHC6} N=8 mice)

C) Flow cytometric analysis of neutrophils (CD11b$^+$, Ly6g$^+$) as a percentage of the CD45$^+$ cells in Panx1$^{fl/fl}$ and Panx1^{MyHC6} hearts after 14-days of isoproterenol treatment. Representative plots of the identified neutrophils from Panx1$^{fl/fl}$ and Panx1^{MyHC6} mice hearts. (Panx1$^{fl/fl}$ N=8, Panx1^{MyHC6} N=8 mice)

D) Representative confocal micrographs of Ly6g staining at 60X from Panx1$^{fl/fl}$ and Panx1^{MyHC6} mice treated with isoproterenol for 14 days. Ly6g was used to stain neutrophils; DAPI was used as a nuclear stain. Quantification of number of neutrophils, Ly6g$^+$ puncta, per 60X field in whole heart tissue from Panx1$^{fl/fl}$ and Panx1^{MyHC6} mice after 14-days of isoproterenol treatment. (Panx1$^{fl/fl}$ N=8, Panx1^{MyHC6} N=9 mice, 3-5 images per mouse averaged)

E) Flow cytometric analysis of macrophages (CD11b$^+$, F4/80$^+$) as a percentage of CD45$^+$ cells from Panx1$^{fl/fl}$ and Panx1^{MyHC6} hearts after 14-days of isoproterenol treatment. Macrophages expressing the co-stimulatory activation marker (CD86$^+$) and macrophages

expressing the anti-inflammatory marker ($CD163^+$, $CD86^-$) as a percentage of the macrophages ($CD11b^+$, $F4/80^+$). Flow cytometric analysis of dendritic cells (DC) ($CD11b^+$, $CD24^+$) as a percentage of $CD45^+$ cells from $Panx1^{fl/fl}$ and $Panx1^{MyHC6}$ hearts after 14-days of isoproterenol treatment. ($Panx1^{fl/fl}$ N=6, $Panx1^{MyHC6}$ N=6 mice)

Data represented as mean $\pm$ SEM. Significance determined using Welch's t-test (B, C, D, E) was used for comparison between two groups. ns = not significant. See also S6 in reference to figure 6.